Journal of Atmospheric and Terrestrial Physics, Vol. 47, No. 1, pp. 243–264, 1985.
Printed in Great Britain.

0021-9169/85 $3.00 + .00
Pergamon Press Ltd.

Neutral air turbulence in the upper atmosphere observed during the Energy Budget Campaign

E. V. THRANE, Ø. ANDREASSEN, T. BLIX, B. GRANDAL
Norwegian Defence Research Establishment, PO Box 25, N-2007 Kjeller, Norway

A. BREKKE
University of Tromsø, PO Box 953, N-9001 Tromsø, Norway

C. R. PHILBRICK
Air Force Geophysics Laboratory, Hanscom AFB, MA 01731, U.S.A.

F. J. SCHMIDLIN
NASA Wallops Flight Center, Wallops Island, VA 23337, U.S.A.

H. U. WIDDEL
Max-Planck-Institut für Aeronomie, Postfach 20, Katlenburg-Lindau, F.R.G.

U. VON ZAHN and F. J. LÜBKEN
University of Bonn, Nussallee 12, 5300 Bonn 1, F.R.G.

(*Received for publication* 29 *August* 1984)

Abstract—A number of different experimental techniques employed in the campaign provided measurements on the fine scale structure of the upper atmosphere, from which information about turbulent intensity, eddy transport and eddy dissipation rates may be extracted. The turbulent state of the mesosphere was shown to be highly variable and significant differences were found between observations obtained during the four salvoes launched during different degrees of geomagnetic disturbance.

1. INTRODUCTION

The Energy Budget Campaign represents a concerted effort to study the energetics of the upper atmosphere. The present paper deals with observations relevant to the study of turbulence in the mesosphere and lower thermosphere.

Two of the aims of the Energy Budget Campaign were to study the nature of turbulence and the role of turbulent energy transport in the upper atmosphere. The present paper describes the combined results of a series of different rocket and ground-based experiments designed to measure parameters relevant to the turbulent flows in the mesosphere and lower thermosphere.

The results clearly show that this part of the atmosphere has at times a very complex temperature and wind structure, with regions of strong turbulence. The rocket experiments were made at the Andøya Rocket Range and Esrange and were supported by ground-based partial reflection measurements in Tromsø. The observations were concentrated in four 'salvoes' launched during different degrees of geomagnetic disturbance: the C-salvo on 11 Nov. 1980 (undisturbed); the B-salvo on 16 Nov. 1980 (moderately disturbed); the A1-salvo on 28 Nov. and the A2-salvo on 1 Dec. 1980 (both strongly disturbed).

2. EXPERIMENTAL METHODS

The details of the different experimental techniques are described by OFFERMANN and THRANE (1981) and here only the basic principles of the methods will be mentioned.

2.1. *The electrostatic ion probe experiment*

The principle of this method rests upon the assumption that positive ions in the lower ionosphere may be regarded as passive tracers for fluctuations in the neutral gas (HILL and BOWHILL, 1976; THRANE and GRANDAL, 1981). It is implicit in this assumption that the lifetime of an ion against recombination is longer than the lifetime of the turbulent eddies of interest in this study.

The ion density fluctuations in the lower ionosphere were measured with high time resolution and accuracy by means of gridded spherical electrostatic probes. For

the Energy Budget Campaign two versions of the probes were flown; three payloads (code-named E4) carried a single probe mounted at the front of the payload; three payloads (code-named E1) carried two probes which were ejected simultaneously from the 'mother' payload during flight. In the latter case the two free-flying dropsondes were ejected sideways, in opposite directions, and moved slowly away from the 'mother' payload during flight, thus providing the opportunity of studying horizontal as well as vertical structures. The experiment and some results have been described by THRANE and GRANDAL (1980), GRANDAL *et al.* (1981) and THRANE *et al.* (1981). The ion current observed throughout the flight at time t may be approximated by

$$I(t) = eN_i(t)\sigma v_R(t) \tag{1}$$

where e is the ionic charge, N_i the positive ion number density, σ an effective probe cross section and v_R the rocket or probe velocity. Since $v_R \sim 1200$ m s^{-1} is normally much larger than the thermal velocity of the ions (~ 400 m s^{-1}), the observed time variations in ion current $I(t)$ may be interpreted as spatial variations of ion density $N_i(h)$. When the trajectory is known, time t may be replaced by height h (or, more precisely, by a distance s along the rocket trajectory). The sampling rates were 1502.4 Hz (E4 probe) and 2000 Hz (E1 probe), providing a spatial resolution of better than 1 m along the trajectories.

An absolute value of the ion density $N_i(t)$ can only be determined from the observed current I if the effective probe cross-section σ is known, but the fluctuation of N_i, ΔN_i, relative to a reference value N_{iref} may be studied without this knowledge. In the following we assume that both the cross-section σ and the rocket velocity v_R vary slowly with time, so that for a limited height interval we may write

$$\frac{\Delta N_i}{N_{iref}} = \frac{\Delta I}{I_{ref}}. \tag{2}$$

The fluctuation ΔN_i and the reference value N_{iref} must be defined with care in order to minimize the effects of spin modulation and of the large scale, rapid increase of the ion density N_i with height. We divide the data into segments of 2048 observations, each segment then corresponds to a height interval of about 1 km. For each segment the large scale slope, the spin modulation and its first harmonic are determined by introducing a function

$$N_{ifit}(t) = a_1 + a_2 t + a_3 \sin \omega t + a_4 \cos \omega t + a_5 \sin 2\omega t + a_6 \cos 2\omega t. \tag{3}$$

This form of the function was chosen because the spin modulation was prominent in the raw data. Here $a_1 \cdots a_6$ are constants determined by a least mean square fit to the data. ω is the angular rocket spin frequency and is accurately known from independent attitude measurements. The fluctuation ΔN_i in ion density is defined as

$$\Delta N_i(t) = N_i(t) - N_{ifit}(t). \tag{4}$$

By subtracting the function N_{ifit} we have minimized contamination by spin modulation and the effects of large scale slope, and the fluctuation $\Delta N_i(t)$ should contain only the physical information of interest. In order to avoid the uncertainty in the effective probe cross section, we need to study the fluctuation $\Delta N_i(t)$ relative to a smoothly varying reference value $N_{iref}(t)$. We choose to define

$$N_{iref}(t) = a_1 + a_2 t, \tag{5}$$

which reflects a least mean square fit to a linear variation of the ambient ion density over the limited height range within each data segment. The relative fluctuation, which is the basis for further analysis, is therefore

$$\frac{\Delta N_i}{N_{iref}}(t) = \frac{N_i(t) - N_{ifit}(t)}{N_{iref}(t)}. \tag{6}$$

The next step is to derive the relative fluctuations in neutral gas number density n, $\Delta n/n_{ref}$, using our initial assumption that the ions are passive tracers for fluctuations in the ambient atmosphere. For each data segment we write (THRANE and GRANDAL, 1981)

$$\frac{\Delta n}{n_{ref}}(t) = F \frac{\Delta N_i}{N_{iref}}(t), \tag{7}$$

where the conversion factor F is assumed constant over the segment and is given by

$$F = \frac{\dfrac{\gamma H_p}{H_n} - 1}{\dfrac{\gamma H_p}{H_i} - 1}. \tag{8}$$

Here γ is the ratio of specific heats ($c_p/c_v = 1.4$ for air). H_p, H_n and H_i are the scale heights for atmospheric pressure, neutral number density and ion number density, respectively. The two former are derived from independent measurements by means of meteorological rockets launched during the campaign (see Appendix 1), whereas the latter is derived directly from the ion probe measurements. Figure 1 shows the factor F versus height derived for the three salvoes.

A Fast Fourier Transform algorithm (SINGLETON, 1969) is then applied to the function $\Delta N_i/N_{iref}(t)$ to provide a power spectrum $P(f)$ of the irregularities. The

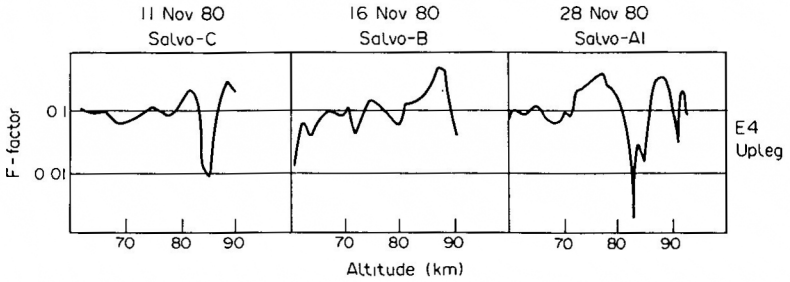

Fig. 1. The conversion factor F computed for each of the three first salvoes, using the atmospheric parameters given in Appendix 1 and ion density scale heights for the E4 ion probes.

root-mean-square (RMS) intensity of the ion density fluctuations and the spectral slope ξ are derived from the spectral analysis and used to estimate the relative fluctuations in neutral number density

$$\left(\frac{\Delta n}{n_{\text{ref}}}\right)_{\text{RMS}} = F\left(\frac{\Delta N_i}{N_{i\text{ref}}}\right)_{\text{RMS}}. \tag{9}$$

The RMS values represent integrals over the spectral range 4–100 Hz, which is believed to correspond roughly to the inertial subrange in the mesosphere.

Finally, estimates of the energy dissipation rate ε and the eddy diffusion coefficient K were derived from the intensity of neutral density fluctuations. This derivation was based upon the following argument: within the inertial subrange of turbulence, all atmospheric density fluctuations are assumed to be caused by forced adiabatic vertical displacements of air parcels. A relative number density fluctuation may then be expressed as

$$\frac{\Delta n}{n_{\text{ref}}} \simeq \left[\frac{1}{H_n} - \frac{1}{\gamma H_p}\right] z, \tag{10}$$

where $z \ll H_p$ and H_n. z is the vertical displacement of the air parcel (see THRANE and GRANDAL, 1981). This density fluctuation represents a potential energy per unit mass

$$E_{\text{pot}} = -g\frac{\Delta n}{n_{\text{ref}}} z \simeq -g\left(\frac{\Delta n}{n_{\text{ref}}}\right)^2 \left[\frac{1}{H_n} - \frac{1}{\gamma H_p}\right]^{-1}. \tag{11}$$

We now assume that this potential energy has been converted from an initial kinetic energy per unit mass

$$E_{\text{pot}} = C_E \tfrac{1}{2} u^2, \tag{12}$$

where C_E is a constant and u is the initial velocity of the element. In other words, for turbulence in the inertial subrange the total energy per unit mass comprises a kinetic and a potential energy. Within this range there is no source and no loss of energy and it seems reasonable to assume that, on the average, there is an equipartition between the kinetic and potential energy, so that

$$\overline{E_{\text{pot}}} = \overline{C_E \tfrac{1}{2} u^2}, \tag{13}$$

where $C_E = 1$ and the bars indicate averaging over the height interval we consider. Later we use $C_E = 1$ in the numerical computations, but for reference we include the constant in the subsequent equations. We now combine equations (10), (11) and (13) and use the conversion factor F to obtain

$$\overline{C_E \tfrac{1}{2} u^2} = \overline{E_{\text{pot}}} = -g\frac{\left[\gamma\frac{H_p}{H_n} - 1\right]}{\left[\gamma\frac{H_p}{H_i} - 1\right]^2} \gamma H_p \left(\frac{\Delta N_i}{N_{i\text{ref}}}\right)^2_{\text{RMS}}. \tag{14}$$

This formula allows us to estimate the mean square turbulent velocity $\overline{u^2}$ from measurements of relative ion number density fluctuations

$$\left(\frac{\Delta N_i}{N_{i\text{ref}}}\right)_{\text{RMS}}.$$

Once the mean square velocity $\overline{u^2}$ is found, the energy dissipation rate ε and the eddy diffusion coefficient K may be derived. In text books on turbulence (see for example TENNEKES and LUMLEY, 1972), dimensional arguments lead to expressions for the energy dissipation rate $\varepsilon \sim u^3/L$ and the eddy diffusion coefficient $K \sim uL$. Here L may be defined loosely as the largest size of a turbulent eddy or as a transition scale between a regime of large scales where buoyancy forces dominate and an inertial subrange where turbulence dominates. For quantitative estimates more precise definitions of ε and K are needed. Attempts to quantify the relations are quoted in the literature (see for example WEINSTOCK, 1978a,b, 1981; ZIMMERMANN and MURPHY, 1980; LILLY *et al.*, 1974). These estimates seem to be uncertain and different answers are given by the different authors. In the following we have chosen to

follow WEINSTOCK (1981) and we use the expression for the energy dissipation rate

$$\varepsilon = 0.4\,\overline{u_Z^2}\,\omega_B, \tag{15}$$

where u_Z is the vertical component of the turbulent velocity ($u^2 = 3u_Z^2$ for isotropic turbulence). Here ω_B is the angular Brunt–Väissällä frequency and we derive ω_B from temperature profiles observed by meteorological rockets during the campaign (see Appendix 1). The eddy diffusion coefficient is given by WEINSTOCK (1978b) as

$$K = 0.8\frac{\varepsilon}{\omega_B^2}. \tag{16}$$

Weinstock's work is based upon theoretical considerations and is supported by observations in the stratosphere. Although we recognize the inherent difficulties in such work, we feel that the above estimates are the best available at the present time.

2.2. *The BUGATTI mass spectrometer experiment*

The Bonn University Gas Analyzer for Turbulence and Turbopause Investigations (BUGATTI) aims at the measurement of absolute number densities of N_2 and Ar with high time resolution and precision. During each of two experiments discussed in this paper (payloads E4 of salvoes B and C) the densities of N_2 and Ar were sampled simultaneously by a double-focusing magnetic spectrometer, details of which have been described by WIRTH and VON ZAHN (1981). The data were taken on the downlegs of the rocket-flights between 125 and 100 km altitude at an effective rate of 94 samples s^{-1}. This rate corresponds to an altitude resolution of 7 m at 100 km height and a time resolution of ~ 10 ms. The latter is close to the time constant with which the BUGATTI ion source follows ambient density fluctuations.

Here we will concentrate on an analysis of the small scale N_2 density fluctuations observed by the BUGATTI instruments. We make the assumption that the N_2 densities n_s inside the ion source faithfully followed the corresponding density fluctuations in the ambient atmosphere n_a. Hence we perform our spectral analysis directly on the ion source densities n_s, without regard for the (slowly varying) ram factor.

Before a spectral analysis of the observed fluctuations was performed, the following three effects have been removed from the raw data:

the regular altitude gradient of the ambient density n_a;
the modulation of the ion source densities n_s due to the nutation of the spinning payload;
a small modulation of the electrometer zero line with the spin frequency ω of the payload.

For this purpose the data stream n_s was broken into sections of about 5 s length and each was individually least-squares-fitted with functions of the form

$$n_{\mathrm{ref}}(t) = \sum_{n=0}^{3\text{ or }4} a_n t^n + \sum_{m=0}^{2} (b_m t^m \sin \omega t + c_m t^m \cos \omega t), \tag{17}$$

where the spin frequency ω is assumed constant. The relative density fluctuations were then calculated from the densities n_s and n_{ref} by

$$\Delta n/n_{\mathrm{ref}} \equiv \frac{n_s - n_{\mathrm{ref}}}{n_{\mathrm{ref}}} \tag{18}$$

This procedure dampens any spectral components in $\Delta n/n_{\mathrm{ref}}$ having periods longer than about 3 s (or 2.5 km near 100 km altitude), regardless of whether these wave components may be of genuine geophysical origin or an artifact of the variable instrument aspect angle. In particular, density variations with the nutation period (about 12 s for both payloads) are essentially eliminated from our relative density fluctuations.

Because the data is collected in the form of a regular time series, the power spectrum $P(f)$ of $\Delta n/n_{\mathrm{ref}}$ is first calculated in terms of the frequency f. It is obtained from the Fourier transform of the autocorrelation function, using the subroutine FTFREQ from IMSL LIBRARIES INC. (1982). The experiment measures, however, the *spatial* spectrum of turbulent structures, because the gas analyzer traverses the medium with a velocity which is orders of magnitude higher than typical turbulent velocities. Hence, in a second step the power spectrum of $\Delta n/n_{\mathrm{ref}}$ was converted to a spatial spectrum $P(\lambda)$, with $\lambda = v_R/f$, where v_R is the rocket velocity. The RMS intensity of $\Delta n/n_{\mathrm{ref}}$ and the slope ξ of the power spectrum $P(\lambda)$ were derived from the spectral analysis.

The relative density fluctuations $\Delta n/n_{\mathrm{ref}}$ presented below are not only due to ambient density fluctuations, but contain a certain amount of noise of instrumental origin. The sources of this noise are small fluctuations of the zero line of the electrometers used for ion detection and the statistical fluctuations in the current sensed by the electrometers. A quantitative analysis of these instrumental contributions is in progress and will be published as soon as completed. Hence, in the following $\Delta n/n_{\mathrm{ref}}$ and the slope ξ of the power spectra are shown as obtained, without any corrections for instrumental noise in the data.

2.3. *The falling sphere accelerometer experiment*

The Energy Budget accelerometer falling sphere experiment has been described by PHILBRICK *et al.* (1981). The 25 cm diameter spheres were instrumented with highly accurate piezoelectric accelerometers and

were released from the mother payload at 65 km altitude. The accelerometers permitted the determination of the motion of the sphere in three dimensions and thus provided information on atmospheric wind structure transverse to the trajectory velocity vector, as well as atmospheric density structure causing drag along the trajectory. The upleg data provides most of the information on the wind velocity and the downleg data provides the density.

The density ρ is determined from the equation for the atmospheric drag force

$$\rho = \frac{2a_D m}{v^2 C_D A}, \tag{19}$$

where a_D is the measured drag acceleration, v the velocity, m and A the mass and cross-sectional area of the sphere and C_D the experimentally determined drag coefficient. The acceleration is determined 12 times per s, providing a spatial resolution of about 100 m in the mesosphere. The atmospheric temperature structure is determined by integration of the hydrostatic equation over a height interval z_1 to z_2,

$$T_{M_2} = T_{M_1}\frac{\rho_1}{\rho_2} - \frac{M}{\rho_2}\frac{g}{k}\int_{z_1}^{z_2} \rho \, dz. \tag{20}$$

T_M is the molecular scale temperature, related to the kinetic gas temperature $T = T_M M/M_0$, where M and M_0 are the mean molecular weights at altitude z and ground level, respectively.

The measurements of temperature and wind structure may be combined to yield a measure of atmospheric stability. The gradient Richardson number is defined as

$$R_i = \frac{\omega_B^2}{\left(\frac{\partial V}{\partial z}\right)^2} = \frac{\frac{g}{T}\left(\frac{\partial T}{\partial z} + \Gamma_s\right)}{\left(\frac{\partial V}{\partial z}\right)^2}, \tag{21}$$

where $\partial V/\partial z$ is the vertical windshear, ω_B the Brunt–Väissälä frequency and Γ_s the adiabatic lapse rate. $R_i < 0$ indicates hydrostatic instability, whereas the atmosphere is normally considered dynamically unstable when $R_i \leqslant 0.25$.

2.4. *The meteorological rocket sondes*

Two types of rocket sondes were used at Esrange during the EBC. The systems are described by SCHMIDLIN *et al.* (1981, 1985). One of these is the Super Loki Datasonde system, which in flight releases a parachute-borne temperature sensor capable of measuring atmospheric temperature in the height range 20–70 km. The specially designed parachute is tracked by radar and serves as a sensor for horizontal winds. From the measured and suitably corrected temperature profile and a knowledge of the pressure at an initial altitude, the pressure and density profiles may be calculated using the perfect gas law, assuming hydrostatic equilibrium.

The second system is the Super Loki Sphere, an inflatable, passive sphere which is released from the rocket above 90 km altitude and tracked by a high precision radar during descent from 90 to about 32 km. Horizontal winds, as well as density, pressure and temperature, may be derived from the measured descent trajectory. For the data sonde the data are combined with data from conventional radio sondes in the stratosphere to provide the necessary initial conditions for integration to higher altitudes. For the passive sphere it is necessary to assume a model temperature value at the top of the profile to initialize the analysis.

2.5. *The foil cloud experiment*

The principle of this method is the release and tracking of a 'soft' radar target in the upper atmosphere (WIDDEL, 1981). The target consists of a cloud of very light weight radar reflecting foils, cut to form individual resonant dipoles adjusted to the radar wavelength. The foil cloud is released from payload near apogee and is tracked by radar as it slowly falls through the mesosphere (maximum usable height typically 94 km). The very low mass-to area ratio of the foils (3.4×10^{-3} kg m^{-2}) favours detection of turbulent air motions, especially vertical movements (ROSE and WIDDEL, 1969), but might also limit the height range over which a horizontal wind profile can be obtained: strong wind shears with their associated turbulence destroy the spatial confinement of the cloud produced aerodynamically during deployment of the cloud and disperse the foils rapidly. The windshears were computed from the formula

$$S = \sqrt{\left(\frac{\partial v_x}{\partial z}\right)^2 + \left(\frac{\partial v_y}{\partial z}\right)^2}, \tag{22}$$

where v_x and v_y are the zonal and meridional components of the wind.

The accuracy of wind speed derived from the radar tracking data depends upon the quality of the radar, as well as upon the wind speeds themselves. Because the 'tracking noise' (deviations of the actual track from a smoothed curve drawn through the radar track) is usually quite small and rarely exceeds $\pm$20–30 m when a good radar is used, differentiation of the smoothed curve against time can be done at short time intervals. Typical intervals are 5 s if the wind speed does not

change much with time, 1 s when the wind speed changes significantly over a period of, at least, 5–10 s or more. The cloud falls with a velocity of typically 50–100 m s^{-1}, and the wind speed may therefore be determined with a height resolution of a few hundred meters. For low wind speeds (5–30 m s^{-1}) the error in the wind speed is estimated to be of order 0.2–2.5 m s^{-1}. For high wind speeds (90–120 m s^{-1}) the error might amount to 10 m s^{-1}. An estimate for an average error of 10% for medium wind speeds appears to be appropriate and conservative. For the wind shears typical errors are expected to be 20–30%. Of course, these considerations become invalid when the cloud passes a very strong windshear. In most cases the cloud will then be torn up into several parts and radar tracking becomes very difficult, if not impossible. Such situations cause apparent abnormally large accelerations of the cloud and are thus easily detected.

2.6. *The partial reflection experiment*

The partial reflection experiment (PRE) is a well established technique for studies of the lower ionosphere by means of high frequency radio waves transmitted from the ground and backscattered from irregularities in the medium. The PRE facility near Tromsø, Norway, operates at 2.75 MHz and has been described by HAUG *et al.* (1977) and HOLT *et al.* (1980). The operation during the EBC has been described by BREKKE *et al.* (1981). The relation between partially reflected radio waves and turbulent layers in the mesosphere has been extensively discussed in the literature (THRANE *et al.*, 1981, and references therein), however there still seems to be some controversy regarding the mechanism causing the scattering. Thus THRANE *et al.* (1981) from measurements in Tromsø show that the partially reflected signals are consistent with volume scattering from turbulence in the inertial subrange, whereas HOCKING and VINCENT (1982) find that Fresnel reflection from horizontally extended sharp vertical gradients can explain their observations made in Adelaide. In spite of these difficulties it is reasonable, with due caution, to use the presence of partial echoes from a certain height region to indicate the presence of turbulent layers in the mesosphere.

3. THE EXPERIMENTAL PROGRAMME DURING THE ENERGY BUDGET CAMPAIGN

Table 1 lists the experiments which provided information on turbulence during the four salvoes of the EBC. In addition, the meteorological rocket systems and the partial reflection experiment were operational before and between the salvoes. The table illustrates that the data are spread in time and space and one can hardly hope to derive a complete picture of the turbulent state of the upper atmosphere during the campaign. Nevertheless, the data from so many different techniques offer an interesting opportunity to search for the characteristics of turbulence near and below the turbopause. We have chosen to concentrate the present study first on the data from the individual

Table 1. Experiments supplying information on atmospheric turbulence in the height ranges indicated

Rocket code and launch location	Experiment	Salvo C 11 Nov. 80	Salvo B 16 Nov. 80	Salvo A1 28 Nov. 80	Salvo A2 1 Dec. 80
E1 Andøya	Twin ion probes (NDRE) ejected from mother payload	001212 UT 60–150 km	033112 UT 73–140 km	032448 UT 61–146 km	
E4 Andøya	Ion probe (NDRE)	001200 UT 62–124 km	033100 UT 60–125 km	032436 UT 55–97 km	
	$[N_2]$ and [Ar] mass spectrometer (University of Bonn)	100–124 km	100–125 km		
E6 Esrange	Falling sphere accelerometer (AFGL)		044700 UT 52–140 km		000900 UT 55–150 km
E7 Andøya Esrange	Foil cloud (Max-Planck-Inst für Aeronomie, Lindau)	003200 UT 94–73 km	034600 UT 86–72 km 054000 UT 97–86 km		
E9 Esrange	Robinsphere Datasonde (AFGL and NASA)	4 launches 20–85 km	5 launches 20–85 km	4 launches 20–85 km	4 launches 20–85 km
Ground-based Tromsø	Partial reflections (University of Tromsø)	70–90 km	70–86 km	65–80 km	

salvoes, comparing the results from different techniques, and then on a comparison of conditions observed during the salvoes.

4. EXPERIMENTAL RESULTS

This section will present selected representative data obtained from the four salvoes: the C-salvo 11 Nov., the B-salvo 16 Nov., the A1-salvo 28 Nov. and the A2-salvo 1 Dec. 1980.

4.1. *The C-salvo*

The C-salvo was launched during geomagnetically undisturbed conditions on 11 Nov. 1980 and, as shown in Table 1, includes 7 rocket flights of particular interest to this study.

The rockets, code-named E4 and E1, both carried ion probes and were launched 12 s apart along parallel trajectories and passed the 100 km altitude level at the same time.

The ion density profile was typical for quiet night conditions with a near exponential increase from 80 to 100 km and a nearly constant value in the height range 100–150 km. The intensity of ion density fluctuations was measured with three instruments. The two dropsondes gave excellent data on both up- and downleg, so that a total of five measurements are available of the height variation of ion density fluctuations. The probes mounted on the E4 payloads do not yield reliable measurements on the downleg parts of the trajectories due to wake effects.

Figure 2 shows the ion density versus height for the three instruments. The data are averaged over 1 km height intervals and constant effective cross-sections σ have been used. These cross-sections have been found by normalizing the ion density at 100 km to the electron density measured at this altitude by means of Faraday rotation techniques (FRIEDRICH *et al.*, 1983). The profiles show some structure with scales of 1–10 km, both in the *D*- and *E*-regions. The large scale slopes in the *D*-region are different for the E1 and E4 payloads. This is probably because the effective cross section changes with height in a different manner for the dropsondes and the fixed probe.

Figure 3 shows an example of a spectrum of fluctuations derived from a data-string of 2048 points (about 1 km) near 77 km. From such spectra the fluctuation intensity and the spectral slope have been derived. The spectral slope is determined in the range 4–100 Hz, corresponding to spatial scales of ~400–10 m. In the mesosphere this scale range should normally be in the inertial subrange of turbulence. Figure 4 shows in the first panel the downleg data (dropsonde no. 2) for ion density fluctuation intensity. Each point represents

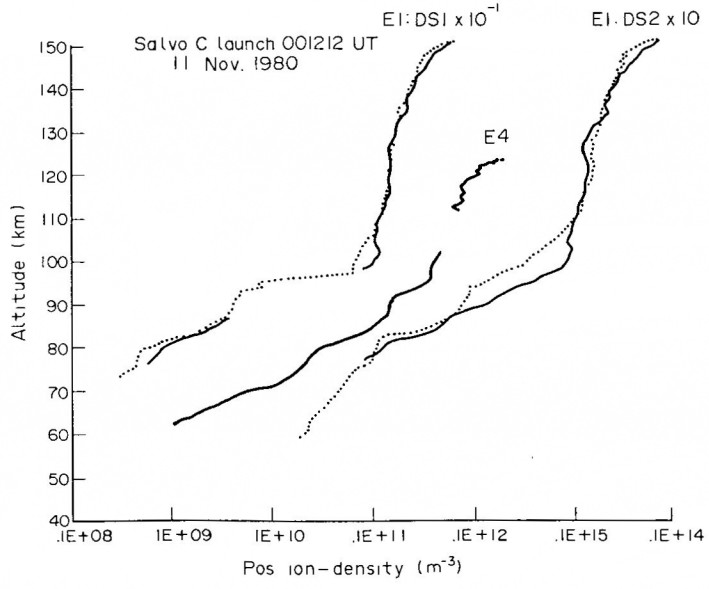

Fig. 2. Ion densities measured at Andøya Rocket Range during the C-salvo. The profiles were measured simultaneously with the fixed ion probe on the E4-payload and with the two free-flying ion probes ejected from the E1-payload (DS1 and DS2). For the two latter probes both upleg (solid lines) and downleg (dotted lines) data are presented.

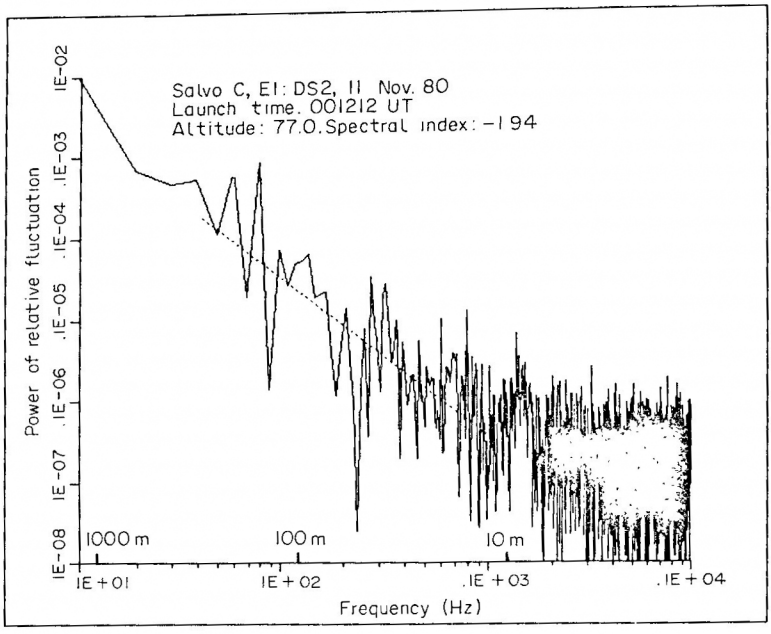

Fig. 3. An example of a power spectrum, from one of the dropsondes (DS2) during the C-salvo, of relative ion density fluctuations $(\Delta N_i/N_{iref})^2$ for a 1 km height interval centered at 77 km. The frequency scale refers to time of flight of the instrument. Using the known payload velocity v_R the frequencies may be converted to length scales $\lambda = v_R/f$, as indicated on the figure.

one spectrum such as that shown in Fig. 3. The data from the other two C-salvo ion probes are very similar to the results in Fig. 4.

In general all the ion probe data indicate the presence of turbulent structures below about 100 km with RMS fluctuation intensities of a few percent and spectral indices near -2 (see Fig. 6). Above 100 km the intensity is small and the spectra flatter, indicating a quiet region with a small noise-like disturbance. All measurements show a layer of strongly fluctuating density near 80 km.

The foil cloud experiment provided detailed information on the mesospheric wind structure below 92 km during the C-salvo at Andøya. The descent velocity of the cloud corresponded well with the velocity expected from the increase in atmospheric density with decreasing height, that is to say there were no strong updrafts or downdrafts along the trajectory. Figure 4 shows in the second panel the total horizontal wind shears derived from the measurements. Several regions with large windshears are observed, near 77, 80, 82 and 85 km. These heights thus indicate regions of possible dynamic instability. The ion probes show enhanced ion density fluctuations in this general height range, in particular the upleg data show a layer with strong fluctuations near 80 km.

Near Tromsø the PRE installation recorded partial echoes in the height range 70–90 km and the electron densities derived from these observations agree well with the rocket measurements at Andøya. (BREKKE *et al.*, 1985). During the C-salvo echoes were most frequently observed from heights near 81, 89 km and 99 km, indicating sharp electron density gradients or scatter from turbulent regions at these heights. Figure 4 shows in the third panel the frequency of occurrence of partial echoes as a function of height.

High quality measurements of the N_2 densities were obtained from the BUGATTI instruments (payloads E4) of the B- and C-salvoes between the apogee of the rocket flight (near 125 km) and the 100 km level. Both payloads exhibited significant nutations, introducing strong modulations in the ion source densities n_s. In order to bring out the genuine small-scale density variations, these experimentally caused modulations had first to be eliminated by the procedure described earlier [see equation (18)].

The relative N_2 density fluctuations (residuals) as calculated from (19) for the C-salvo are shown in the left hand side of Fig. 5. It is notable that throughout the altitude range of measurement these fluctuations stay almost exclusively within the band of $\pm 2\%$ and mostly within $\pm 1\%$. On the right hand side the spectral power vs. frequency (upper abscissa) and vs. wavelength

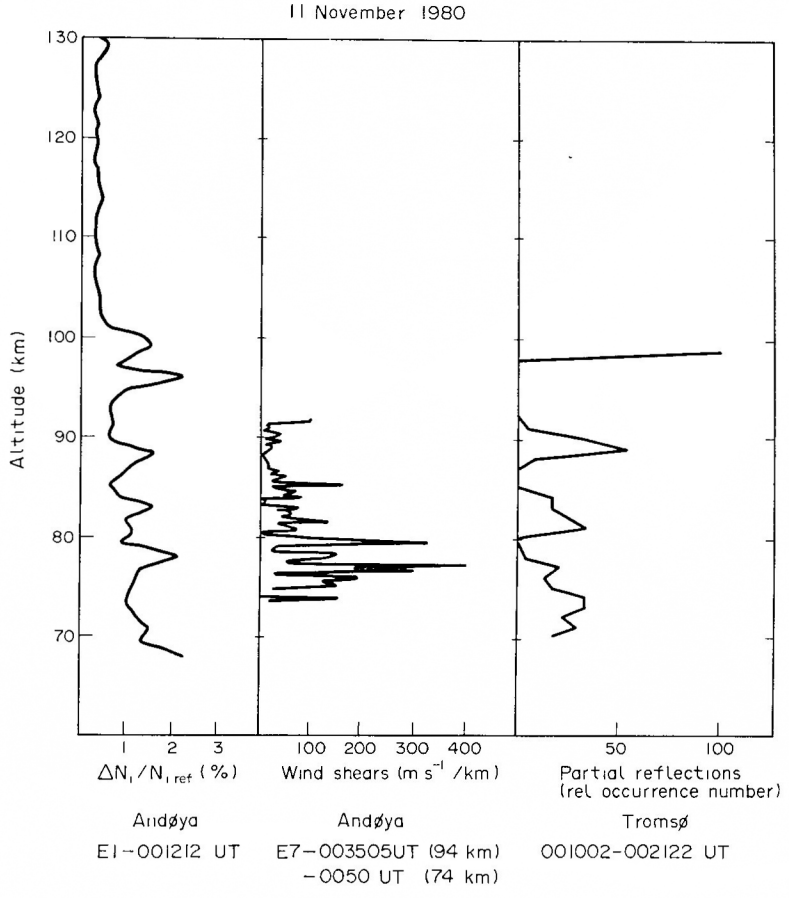

Fig. 4. Some results obtained during the C-salvo (see also Table 1). Left panel: ion density fluctuations $(\Delta N_i/N_{iref})_{RMS}$ in per cent for one of the three ion probes (dropsonde no. 2, downleg). The values represent integration over the power spectrum from 4 to 100 Hz. Middle panel: horizontal wind shears derived from the foil cloud experiment at Andøya. Right panel: frequency of occurrence of partial echoes observed during the E1/E4 flights. The measurements were made by the partial reflection ionospheric radar (PRE) located near Tromsø, 120 km north-east of the Andøya Rocket Range. The radar operates at 2.75 MHz.

(lower abscissa) are shown as calculated for the 4 altitude bins. For an approximate conversion of the power spectrum to wavelength the reciprocal frequencies were multiplied with the total payload velocity at the middle point of the altitude bin.

The power spectra show (expected) peaks near 14 Hz, the first harmonic of the spin frequency. There are also noticeable spikes near 24 hz, of unknown origin. Much more important, however, is the fact that in the altitude region from 96 to 105 km the slope ξ of the power spectra vs. frequency is close to -2 for about 1.5 orders of magnitude in frequency (and wavelength).

The spectral slope ξ as calculated from the spectral power in the frequency band 0.5–10 Hz is shown in Fig. 6 in more detail. In this figure we also show the ion density fluctuations and spectral slopes derived from the ion probe measurements, using the procedure described in Section 2.1.

The BUGATTI results on N_2 densities indicate a spectral slope near -2 for the altitude range 96–102 km. This is in close agreement with the slope derived from the ion density fluctuations. The magnitudes of the fluctuations are also in reasonable agreement. One should remember, however, that the frequency bands analyzed in the 2 experiments are not identical, though overlapping. Above 100 km a gradual flattening of the power spectra is observed and above 120 km an almost white noise spectrum ($n \simeq 0$) is obtained. It should be

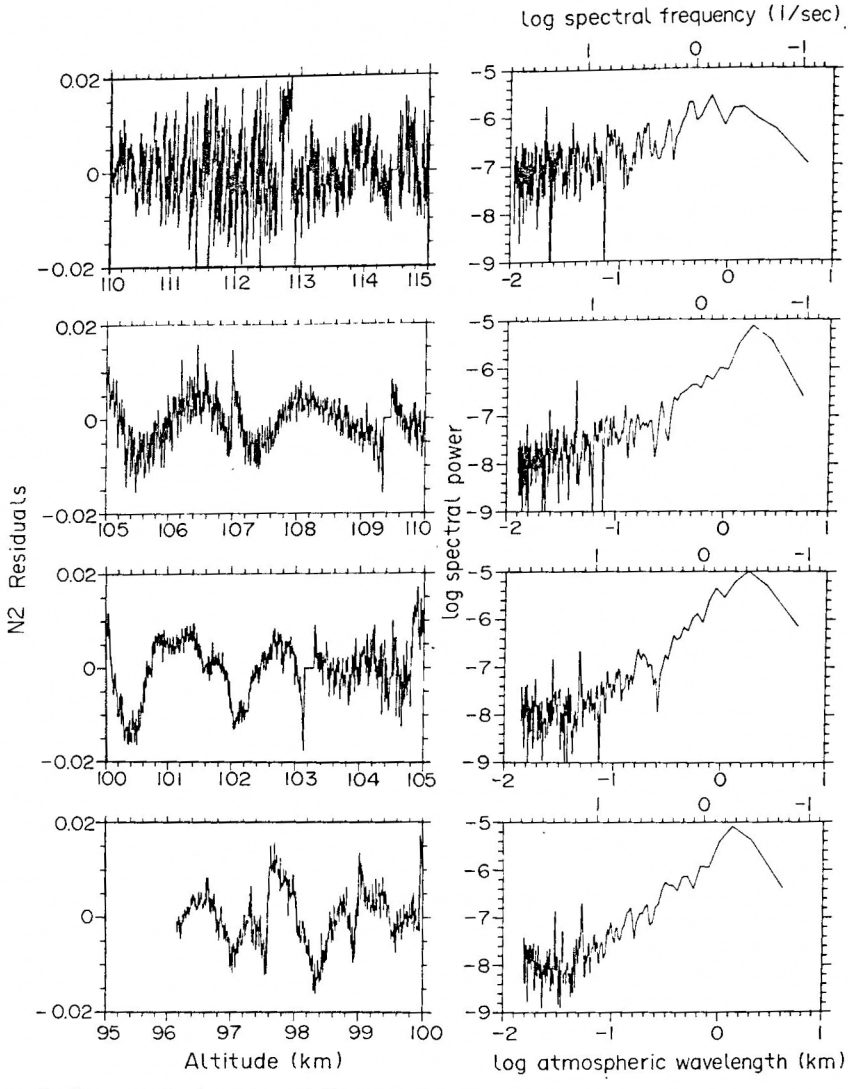

Fig. 5. Results from the C-salvo flight of the BUGATTI instrument. Left panels: the relative N_2 density fluctuations (residuals) as a function of height. Right panels: spectra derived from the data in the left panels.

pointed out that the BUGATTI data were obtained on the downleg of the E4 payload. The ion probe data best suited for comparison were the downleg data for one of the E1 dropsondes. Thus the data in Fig. 6 were obtained on two different payloads. The 100 km level on the downleg was crossed by the two payloads at times which differed by about 50 s and 10 km in horizontal position, and this could account for the differences observed by the two methods.

We interprete the data of Fig. 6 as indicating that at the time of salvo C there existed an extended inertial subrange of neutral air turbulence up to at least 105 km. The inertial subrange is for large scales bounded by the buoyancy range and for small scales by the viscous range. The Kolmogorov microscale which governs the transition to the viscous range increases with altitude, while the scale which marks the transition to the buoyancy range remains relatively fixed. Thus it is theoretically expected that the inertial subrange should disappear at higher altitudes. This transition should not, however, lead to a white noise spectrum at altitudes above 100 km. Therefore we suspect that at altitudes above 100 km the zero spectral index measured by the BUGATTI instrument for scales

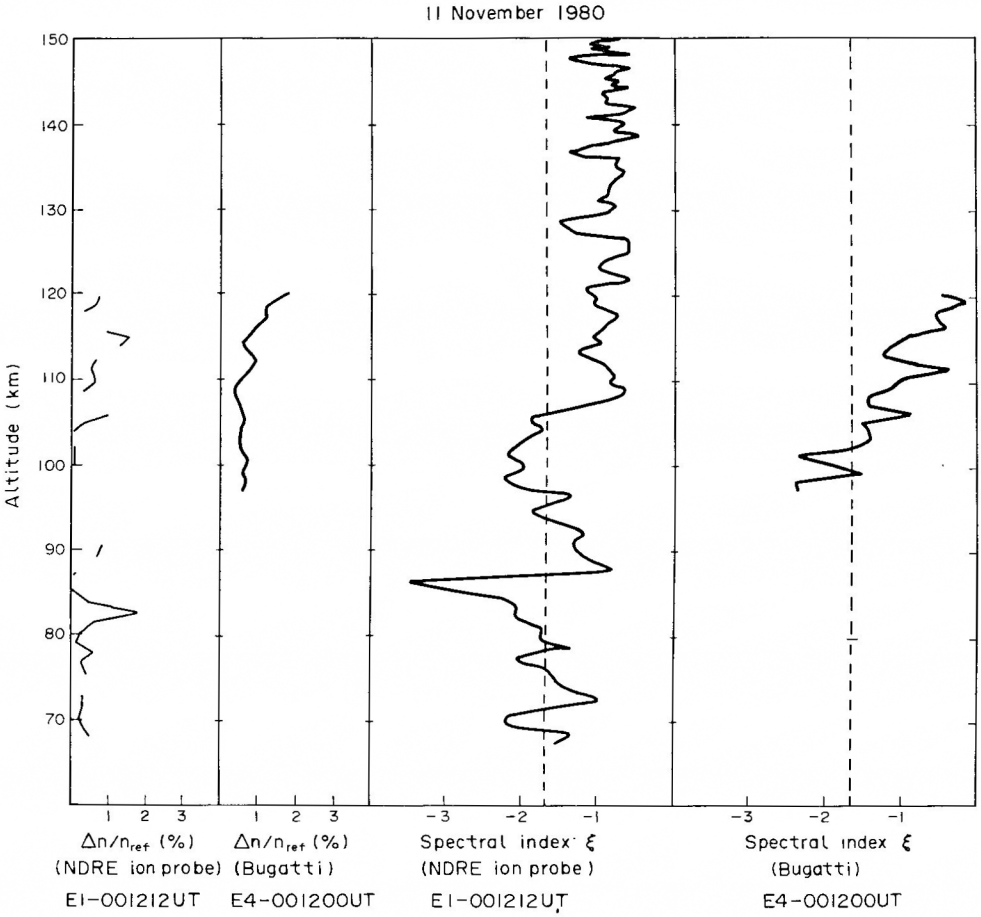

Fig. 6. C-salvo results. Neutral density fluctuation in per cent (dropsonde no. 2, downleg), the relative N_2 density fluctuations $\Delta n/n_{ref}$ in per cent (E4-BUGATTI) and spectral indices ξ derived from the two experiments. The dotted lines indicate a slope of $-5/3$.

below 100 m, as shown in Figs. 5 and 6, is mostly generated by the instrument. As mentioned earlier, this subject is under active study.

In summary, the data obtained in the C-salvo indicate the presence of turbulence in the mesosphere and lower thermosphere up to altitudes of about 108 km. The mass spectrometer and ion probe results are in general agreement in the height region of overlap. In the mesosphere the foil cloud experiment shows a complex wind structure, with strong horizontal shears in the region from 76 to 80 km and near 85 km. The data sondes launched from Esrange during the C-salvo (see Table 1) also show wind and temperature structures in the mesosphere (PHILBRICK *et al.*, 1985). Unfortunately the data were not of sufficiently high quality to allow determination of Richardson numbers.

4.2. *The B-salvo*

The B-salvo was launched on 16 Nov. 1980 during moderately disturbed geomagnetic conditions. One of the ion probe dropsondes on the E1 payload failed completely and the other only worked satisfactorily on the upleg. Figure 7 shows the averaged ion density profiles from the available high quality data. The *D*-region ion densities were about a factor of 10 larger than those measured during the C-salvo and much less structure with scales of 1–10 km was observed. Figure 8 shows that the fine scale fluctuations in the *D*-region were also less intense than during the C-salvo. An interesting feature is the region of strong irregularities in the upper *E*-region. These irregularities have been discussed in a companion paper (DICKINSON *et al.*,

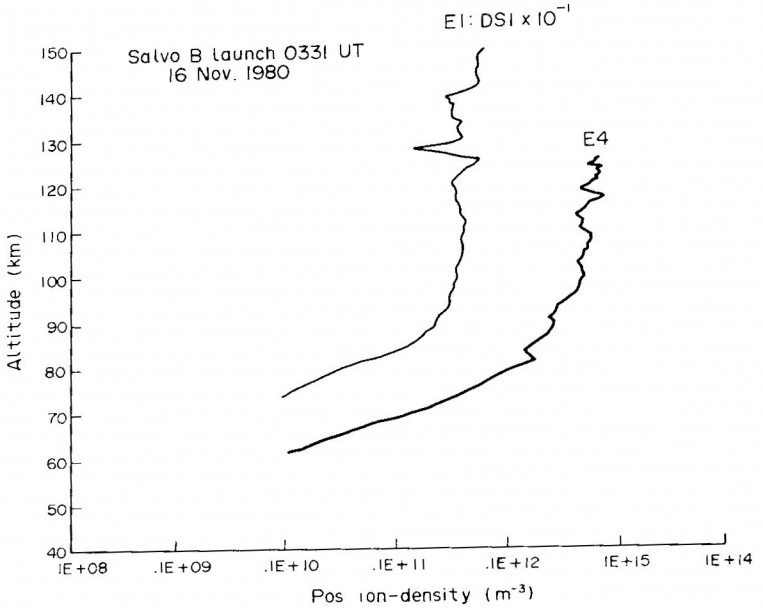

Fig. 7. Ion densities measured at Andøya Rocket Range during the B-salvo. The profiles were measured simultaneously with the fixed ion probe on the E4-payload and with one free-flying ion probe (DS1) ejected from the E1-payload.

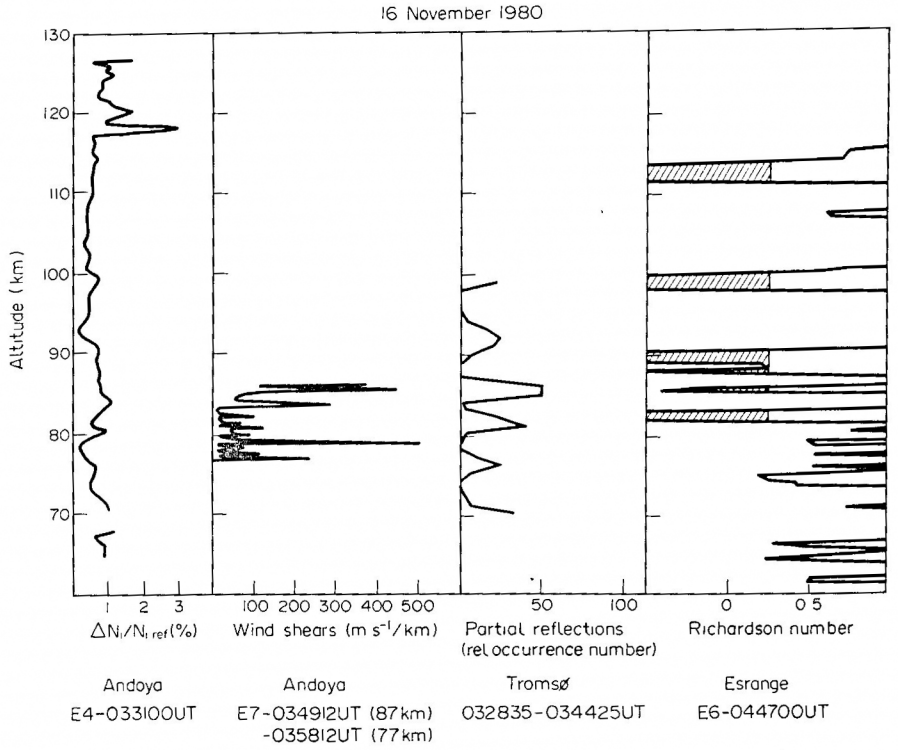

Fig. 8. Some results from the B-salvo. Panels from left to right: ion density fluctuations $(\Delta N_i/N_{i\text{ref}})_{\text{RMS}}$ in per cent (E4 ion probe, upleg). The values represent integration over the spectral range 4–100 Hz; horizontal windshears from the foil cloud experiment; partial reflection occurrence rate measured at the Tromsø PRE facility; Richardson numbers derived from the E6 falling sphere experiments—the hatched areas indicate regions of dynamical instability ($R_i < 0.25$).

1985) and are most likely associated with plasma phenomena. Figure 8 also shows the windshears derived from the foil cloud experiment, the occurrence rate of partial reflections and the Richardson numbers derived from the falling sphere experiment in the E6 payload (see Table 1). The foil cloud experiment indicates strong shears near 79 and 86 km, below 84 km height the shears were in general weaker than those observed on the 11 November. The E6 results indicate a fairly stable mesosphere below about 80 km, but with regions of unstability near 82, 90, 110 and 113 km. The small Richardson's numbers observed in some of these regions may, however, be caused by infrasonic shock waves and these effects are being studied in further detail. In Fig. 9 we show the relative N_2 density fluctuations (residuals) and power spectra obtained from the BUGATTI instrument of salvo B in an identical format as in Fig. 5, except for the fact that now the altitudes studied reach from 100 to 120 km. It is immediately evident that nowhere does there exist a well developed inertial subrange with a slope of $-5/3$ (with respect to a frequency distribution). Furthermore, below 105 km these fluctuations, and consequently the spectral power, is noticeably less than during the salvo C experiment. Both features are in full accordance with the findings of the E1 ion dropsondes.

The spectral slope as determined from the BUGATTI data (again for the frequency band 0.5–

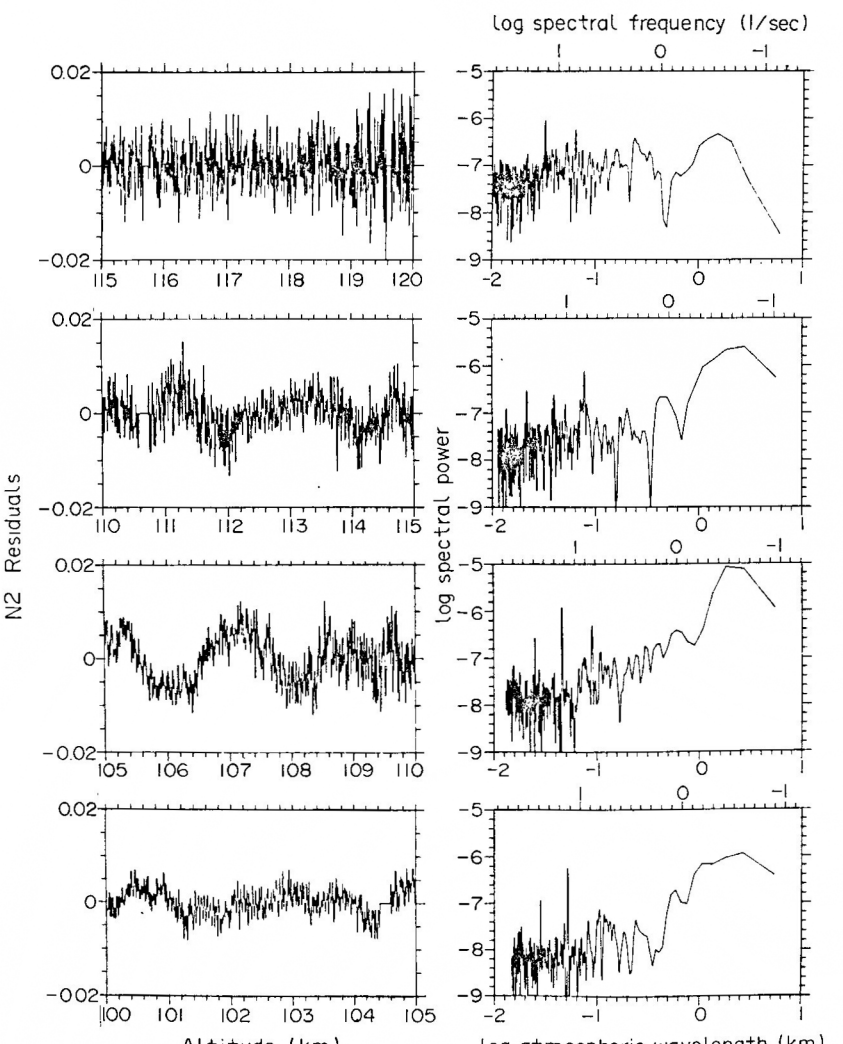

Fig. 9. Results from the B-salvo flight of the BUGATTI instrument. Left panels: the N_2 density fluctuations (residuals) as a function of height. Right panels: spectra derived from the data in the left panels.

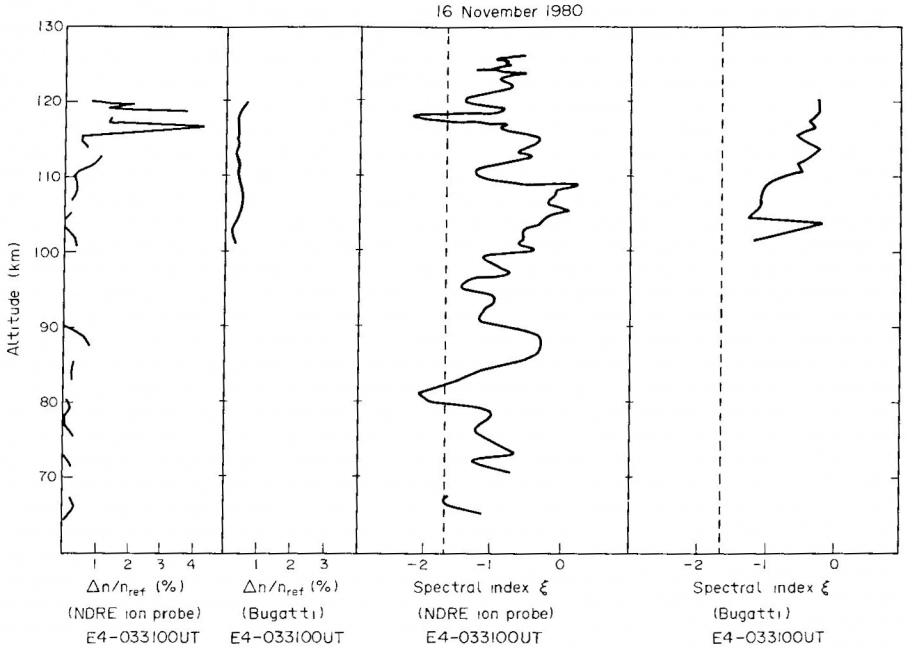

Fig. 10. B-salvo results. Neutral density fluctuations in per cent (E4 ion probe upleg), relative N_2 density fluctuations (residuals) in per cent (E4-BUGATTI) and spectral indices ξ derived from the two experiments. The dotted lines indicate $\xi = -5/3$.

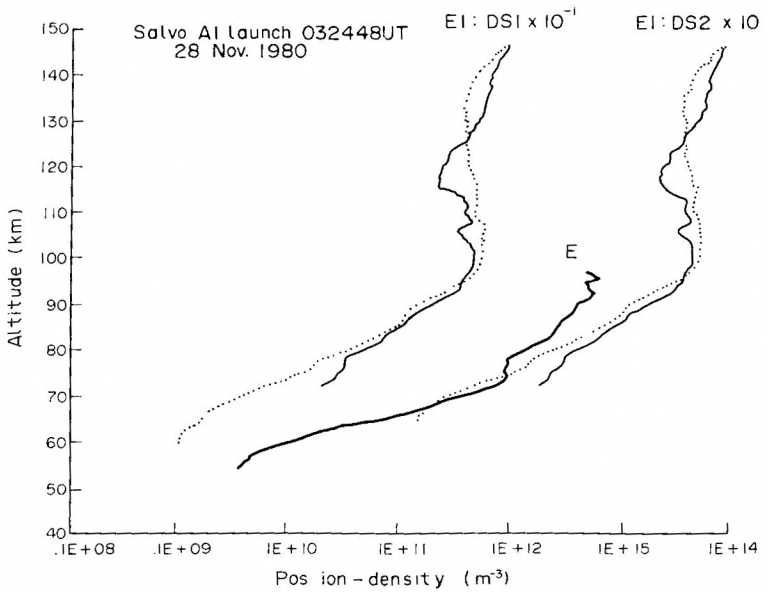

Fig. 11. Ion densities observed at Andøya Rocket Range during the A1-salvo. The profiles were measured simultaneously with the fixed ion probe on the E4-payload and with the two free-flying ion probes ejected from the E1-payload (DS1 and DS2). For the two latter probes both upleg data (solid lines) and downleg data (dotted curves) are shown.

10 Hz) changes from $\xi \sim -1$ near 100 km towards $\xi \sim 0$ near 120 km altitude (see Fig. 10). With reference to our discussion of the salvo C results we emphasize, however, the yet uncertain meaning of this transition towards a white-noise spectrum at high altitudes.

The ion density fluctuation intensities are in general agreement with the BUGATTI results between 100 and 115 km, but above 115 km the strong fluctuations observed with the ion probe are not seen by the BUGATTI instrument. This indicates, as mentioned earlier, that these strong ion density fluctuations are associated with plasma instabilities. The spectral indices ξ for the two experiments also differ significantly at these heights.

The geomagnetic disturbance of the night of 16 November 1980 deposited a moderate amount of energy in the upper atmosphere (OFFERMANN, 1985). The B-salvo results indicate that the neutral air in the mesosphere and lower thermosphere below 100 km was less turbulent than during the C-salvo. The wind measurements by the meteorological rockets at Esrange showed, however, that there were stronger winds and more wave activity in the mesosphere during the B-salvo than during the C-salvo.

4.3. *The A1- and A2-salvoes*

Both the A1-salvo (28 Nov. 1980) and the A2-salvo (1 Dec. 1980) were launched into an atmosphere disturbed by strong geomagnetic storms. Energetic electron precipitation caused enhanced ion densities in the lower ionosphere, as illustrated in Fig. 11 for the A1-salvo. Note that there are irregular structures present in both the *D*- and *E*-regions. Figure 12 shows small scale fluctuation intensities of ion density for one of the E1 dropsondes launched in the A1-salvo and the occurrence rate of partial echoes. All three ion probes launched in this salvo gave good quality data and show the same characteristic picture, i.e. strong fluctuations below about 85 km and very weak fluctuations above this height. The spectral indices support the presence of turbulence below 80–90 km and the rather abrupt change to a noise like spectrum above this height. An example of the raw data is shown in Fig. 13, illustrating the strong irregular structures observed in the 75 km region by the two free-flying ion probes. These fluctuations were the strongest observed during all the flights. Unfortunately no ion probe data are available for the A2-salvo, but the wind structures in the mesosphere are similar on 28 Nov. and 1 December. The Richardson numbers from the A2-salvo are shown in Fig. 14 and indicate the presence of turbulence in the mesosphere. It should be noted (PHILBRICK *et al.*, 1985) that the temperature structure during the A1- and A2-

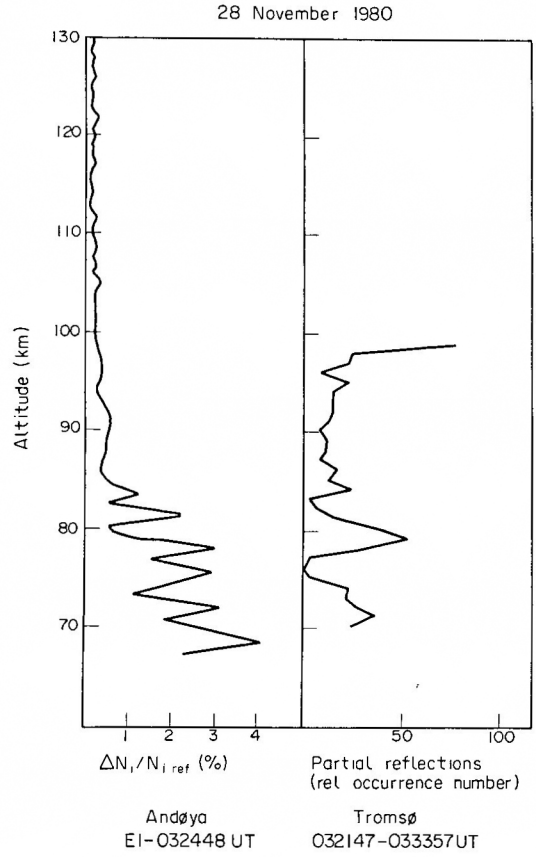

Fig. 12. Some results from the A1-salvo. Left panel: ion density fluctuations $(\Delta N_i/N_{i\text{ref}})_{\text{RMS}}$ in per cent (dropsonde no. 1, downleg). The values represent integration of the power in the spectral range 4–100 Hz. Right panel: the relative occurrence rate of partial reflections measured at the Tromsø PRE facility.

salvoes were quite different from the C- and B-salvo temperatures in that the two disturbed salvoes showed higher temperatures near 80–90 km and no pronounced mesopause.

5. DISCUSSION

The data presented above gives an interesting, although far from complete, picture of the dynamical state of the upper atmosphere during the Energy Budget Campaign. Some conclusions may be drawn at the present stage of the analysis and these will be summarized below. The ion probe results have been carefully analysed according to the procedure outlined in Section 2.1. to give relative fluctuation intensities $\Delta n/n$ of the neutral air, using the conversion factor F shown in Fig. 1. Figure 15 shows the resulting relative

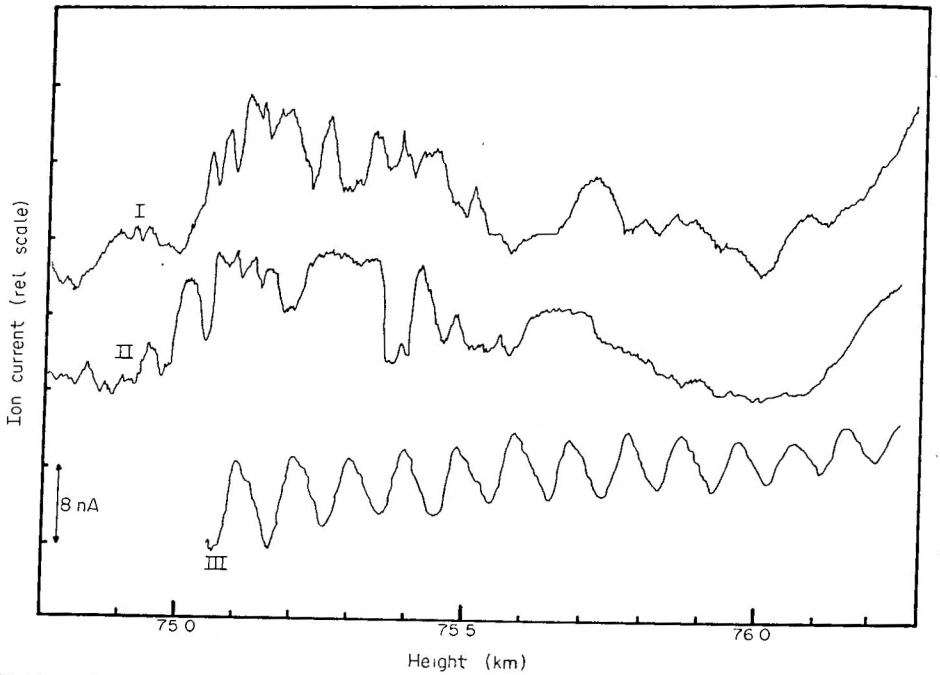

Fig. 13. Examples of ion currents (raw data) measured at three points in space simultaneously during the A1-salvo. I and II indicate measurements made in the two E1 dropsondes, whereas III indicate measurements in the E4 payload. The curves have been shifted in the vertical scale to show the fine structure. The two E1 dropsondes were about 40 m apart in the horizontal direction at the time of measurement, whereas the E4 payload was about 3.6 km away. The E4 probe show pronounced spin modulation in the ion current.

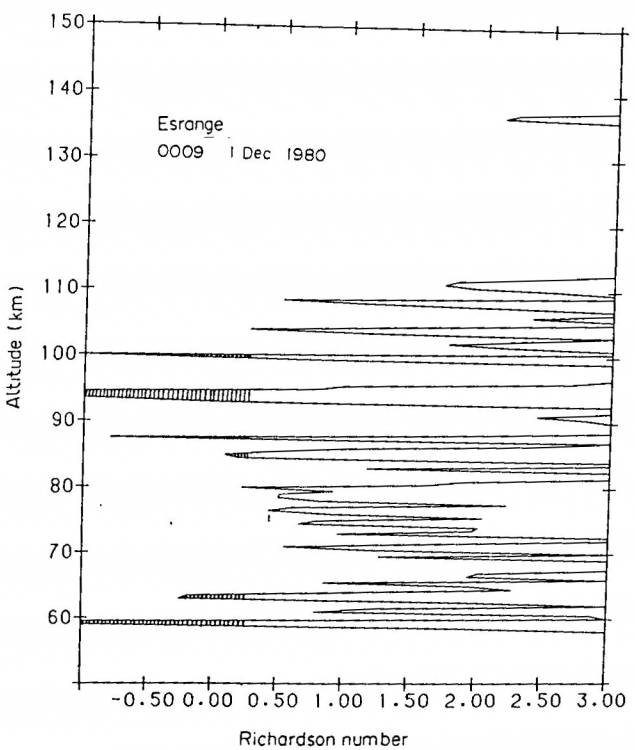

Fig. 14. Richardson numbers derived from the E6 falling sphere experiment during the A2-salvo—the hatched areas indicate regions of dynamical instability ($R_i < 0.25$).

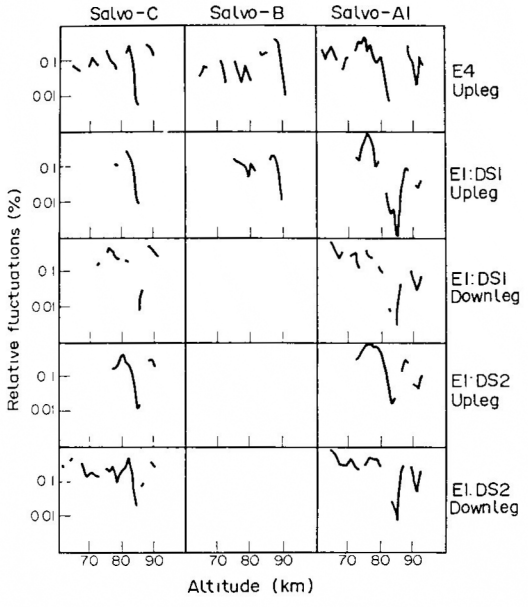

Fig. 15. Relative fluctuations $(\Delta n/n_{\text{ref}})_{\text{RMS}}$ in neutral air number density derived from the ion probes launched in all three salvoes. DS1 and DS2 refer to the dropsondes ejected from the E1 payload.

fluctuation intensity $\Delta n/n_{\text{ref}}$ for the neutral air. Upleg and downleg data are shown separately for all the instruments. The gaps in the curves are due to instrumental uncertainties. In general the RMS fluctuation intensity in the neutral air density is of the order of 0.1%, but there are large variations with height and significant changes from salvo to salvo. The largest fluctuations are observed in the A1-salvo, whereas the B-salvo has the smallest fluctuation intensity. All the curves show a minimum in the fluctuation intensity near the mesopause. Inspection of the meteorological rocket data (see Appendix 1) reveals that the factor

$$F = \frac{\gamma H_p/H_n - 1}{\gamma H_p/H_i - 1} \tag{23}$$

is small at these heights, because $\gamma H_p \approx H_n$, i.e. the atmosphere has a nearly adiabatic temperature gradient. In an adiabatic atmosphere vertical displacements of air cells will not cause large neutral air density perturbations, although they may cause ion density fluctuations. It should be pointed out again that measurements of H_p and H_n in the mesosphere were only available from Esrange and not at the same times as the E1 and E4 launches. At Esrange, however, 4–5 met-rocket flights were available for each salvo. The factor F was therefore calculated from H_p and H_n values derived from several of these flights for each salvo, in order to test its variability. Although the position and depth of the mesopause minimum in F showed some variability, the conclusion was that the changes in F from salvo to salvo were real and significant. We therefore feel justified in using the meteorological rocket data from Esrange in the further analysis of the E1 and E4 results from Andøya.

The RMS turbulent velocities were derived from the data using equation 14. In each salvo the different ion probes yielded consistent results and the data for each salvo were averaged over 5 km height intervals using all probes and both upleg and downleg data, where available. Probable errors were estimated, based upon uncertainties in the data and in the computational procedure. Figure 16 shows the results. Below 80 km there are significant differences between the three salvoes. The A1-salvo, which represents geomagnetically strongly disturbed conditions, also observes strong mesospheric turbulence. Surprisingly, the B-salvo, representing a moderate geomagnetic disturbance, observes the weakest turbulence. Near the mesopause region all salvoes indicate turbulent velocities of the same magnitude, but the error bars are large for the C- and A1-salvoes and hence a meaningful comparison is difficult for this altitude range.

The turbulent energy dissipation rate $\varepsilon = 0.4\,\overline{u_z^2}\,\omega_B$ and the eddy diffusion coefficient $K = 0.8\,\varepsilon/\omega_B^2$ may now be estimated according to the arguments outlined in Section 2.1. The Brunt–Väissälä frequency ω_B has been derived from the met-rocket flights and is given in Appendix 1. Figures 17 and 18 show the estimates of $\varepsilon(h)$

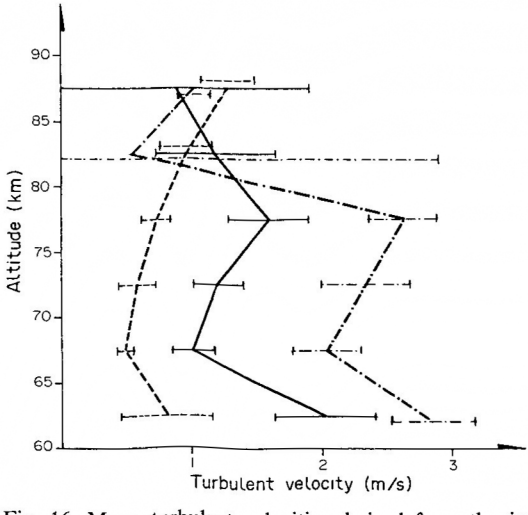

Fig. 16. Mean turbulent velocities derived from the ion probe measurements from three salvoes. —— C-salvo, – – – – B-salvo, –·–·–·–·– A1-salvo.

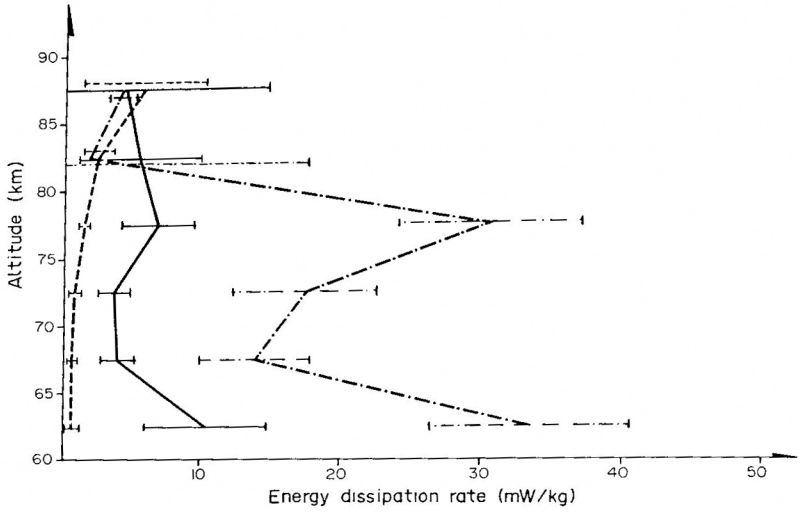

Fig. 17. Energy dissipation rates of turbulence for three salvoes, derived from ion probe measurements. —— C-salvo, – – – – B-salvo, –·–·–·– A1-salvo.

and $K(h)$, respectively, for the three salvoes. Again there are striking differences between the salvoes below 80 km. A study of the wind shears derived from the foil cloud experiment supports the conclusion that the mesosphere below 80 km is more turbulent during the C-salvo than during the B-salvo. On the other hand, the mass spectrometer indicates complete mixing up to about 120 km during the B-salvo, whereas the atmosphere during the C-salvo shows a transition to diffusive equilibrium starting near 100 km (VON ZAHN *et al.*, 1985). A possible explanation for these surprising results may be that the upper atmosphere was well mixed by turbulence at a time before the B-salvo which was sufficiently long to allow the turbulence to die out but not long enough to allow diffusive equilibrium to be re-established.

Figure 18 includes an estimated model of the eddy diffusion coefficient K given in the U.S. Standard

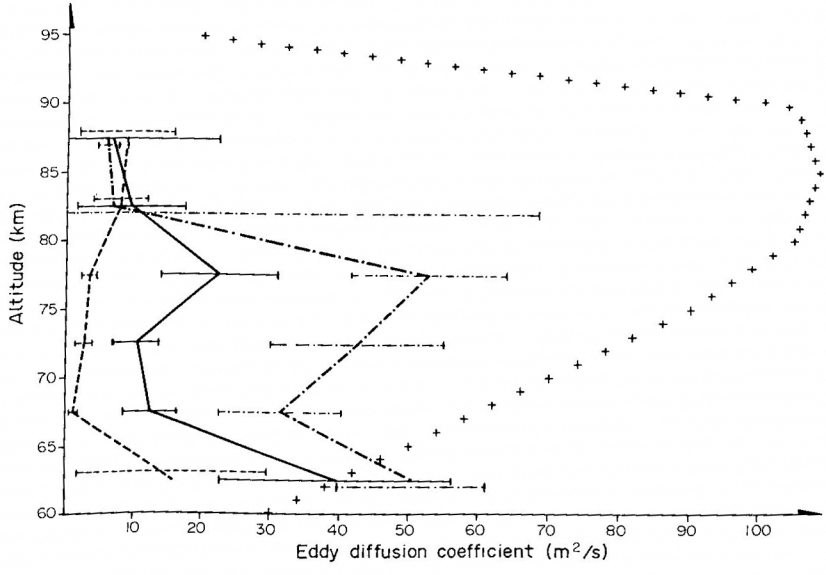

Fig. 18. Turbulent eddy diffusion coefficients for three salvoes, derived from ion probe measurements. —— C-salvo, – – – – B-salvo, –·–·–·– A1-salvo. + + + Values from the U.S. Standard Atmosphere (1976).

Atmosphere (U.S. GOVT. PRINTING OFFICE, 1976). We note that the values of K derived for all three salvoes are less than those given in the Standard. The derivation of K and ε involves, of course, a number of assumptions, and the absolute magnitudes given must be regarded with caution. The works by WEINSTOCK (1978a,b), ZIMMERMANN and MURPHY (1980) and LILLY *et al.* (1974) quote different formulae for estimating ε and K and the statistical errors in our measurements are small compared to the possible systematic errors. Combining these factors we feel that our determination of the energy dissipation rate ε should be correct within a factor of 2. The determination of the eddy diffusion coefficient K is more uncertain and errors of a factor of 3–4 seem possible. We believe, however, that the observed differences between the salvoes are real, since we have analysed all data in a consistent manner, using the same set of assumptions and formulae. When comparing with the U.S. Standard Atmosphere values one should also keep in mind that our results represent instantaneous values of turbulent parameters and the turbulent state of the mesosphere is likely to be very variable.

One should also remember that the standard atmosphere values are based on measurements at middle and low latitudes. It is interesting to note that LINDZEN (1981) has predicted a minimum in the eddy diffusion coefficient near the mesopause at middle and high latitudes. Qualitatively the results from salvoes A and C agree with these predictions.

At the present stage of the analysis it is not possible to determine whether or not a direct relation exists between the energy input during geomagnetic disturbances and the turbulent state of the mesosphere.

Acknowledgement—This research was supported in part by NATO Research Grant No 180.81.

REFERENCES

BREKKE A., HOLT O., DICKINSON P. H. G., FRIEDRICH M., HANSEN T., STAUNING P. and THRANE E. V. 1985 *J. atmos. terr. Phys.* **47,** 101.

BREKKE A., HANSEN T. and HOLT O. 1981 *Energy Budget Campaign 1980*, BMFT-FB-W81-052, OFFERMANN D. and THRANE E. V. Eds, p. 65.

DICKINSON P. H. G., GRABOWSKI R., HANUISE C., MACKINNON D. J., NIELSEN E., THRANE E. V., VILLAIN J. P., WOLF H. and ANDREASSEN Ø. 1985 *J. atmos. terr. Phys.* **47,** 265.

FRIEDRICH M., BAKER K. D., DICKINSON P. H. G., DUMBS A., GRANDAL B., ANDREASSEN Ø., THRANE E. V., SMITH L. G., STAUNING P. AND TORKAR K. M. 1985 *J. atmos. terr. Phys.* **47,** 89.

GRANDAL B., CHRISTENSEN R. and THRANE E. V. 1981 *Energy Budget Campaign 1980*, BMFT-FB-W81-052, OFFERMANN D. and THRANE E. V. Eds, p. 233.

HAUG A., THRANE E. V., BJØRNÅ K., BREKKE A. and HOLT O. 1977 *J. atmos. terr. Phys.* **39,** 1333.

HILL R. J. and BOWHILL S. A. 1976 Aeronomy Report no. 75, University of Illinois.

HOCKING H. W. and VINCENT R. A. 1982 *J. atmos. terr. Phys.* **44,** 843.

HOLT O., BREKKE A. and HANSEN T. 1980 *Proceedings of the Vth ESA PAC Symposium on European Rocket and Balloon Programmes and Related Research*, ESA SP-152, p. 387.

IMSL LIBRARIES INC. 1982 Reference manual, Edn 9. IMSL Inc., Houston, Texas.

LILLY D. K., WACO D. E. and ADELFANG S. I. 1974 *J. appl. Met.* **13,** 488.

LINDZEN R. S. 1981 *J. geophys. Res.* **86,** 9707.

OFFERMANN D. 1985 *J. atmos. terr. Phys.* **47,** 1.

OFFERMANN D. and THRANE E. V. 1981 *Energy Budget Campaign 1980, Experiment summary*, Forschungsbericht W81-052, Bundesministerium für Forschung und Technologie, F.R.G.

PHILBRICK C. R., SCHMIDLIN F. J., GROSSMANN K. U., LANGE G., OFFERMANN D., BAKER K. D., KRANKOWSKY D. and VON ZAHN U. 1983 *J. atmos. terr. Phys.* **47,** 159.

PHILBRICK C. R., MCISAAC J. P., FRYCKLUND D. H. and BUCK R. F. 1981 *Energy Budget Campaign 1980*, BMFT-FB-W81-052, OFFERMANN D. and THRANE E. V. Eds, p. 352.

ROSE G. and WIDDEL H. U. 1969 *Z. Geophys.* **35,** 211.

SCHMIDLIN F. J., PHILBRICK C. R. and OFFERMANN D. 1981 *Energy Budget Campaign 1980*, BMFT-FB-W81-052, OFFERMANN D. and THRANE E. V. Eds, p. 382.

SCHMIDLIN F. J., CARLSON M., REES D., OFFERMANN D., PHILBRICK C. R. and WIDDEL H. U. 1985 *J. atmos. terr. Phys.* **47,** 183.

SINGLETON R. C.	1969	*IEEE Trans. Radio Electroacoustics* **AU-17,** 93.
TENNEKES H. and LUMLEY J. L.	1972	*A First Course in Turbulence.* MIT Press, Cambridge, MA, U.S.A.
THRANE E. V. and GRANDAL B.	1980	*Proceedings of the Vth ESA PAC Symposium on European Rocket and Balloon Programmes and Related Research,* ESA SP-152, p. 61.
THRANE E. V. and GRANDAL B.	1981	*J. atmos. terr. Phys.* **43,** 179.
THRANE E. V., GRANDAL B., FLÅ T. and BREKKE A.	1981	*Nature* **292,** 221.
U.S. GOVT. PRINTING OFFICE	1976	U.S. Standard Atmosphere, NOAA-S/T76-1562. U.S. Government Printing Office, Washington, DC.
WEINSTOCK J.	1981	*J. atmos. Sci.* **38,** 880.
WEINSTOCK J.	1978a	*J. atmos. Sci.* **35,** 634.
WEINSTOCK J.	1978b	*J. atmos. Sci.* **35,** 1022.
WIDDEL H. U.	1981	*Energy Budget Campaign 1980,* BMFT-FB-W81-052, OFFERMANN D. and THRANE E. V. Eds, p. 368.
WIRTH J. and VON ZAHN U.	1981	*Energy Budget Campaign 1980,* BMFT-FB-W81-052, OFFERMANN D. and THRANE E. V. Eds, p. 310.
ZIMMERMANN S. P. and MURPHY E. A.	1980	AFGL-TR-80-0020, Environmental Research Papers no. 691, Hanscom AFB, MA, U.S.A.

APPENDIX 1

This appendix gives the scale heights for pressure (H_p), neutral number density (H_n), ion number density (H_i) and the Brunt-Väisälä frequency ω_B as a function of altitude. H_p, H_n and ω_B were derived from the falling sphere measurements of pressure, neutral density and temperature. H_i was derived from the ion-probe measurements.

(A) *C-Salvo, 11 Nov. 1980*

Altitude (km)	Esrange (E9—015530 UT) H_p (km)	Esrange (E9—015530 UT) H_n (km)	Andøya (E4—001200 UT) H_i (km)	Esrange (E9—015530 UT) ω_B^2 ($\times 10^{-3}$ s^{-2})
60	8.11	8.83	−4.07	0.26
61	7.76	9.69		0.11
62	7.52	7.89		0.35
63	7.56	6.92		0.43
64	7.63	8.27		0.27
65	7.51	7.88		0.31
66	7.80	7.92		0.35
67	7.80	7.68		0.38
68	7.31	7.89		0.25
69	7.21	8.50		0.18
70	7.47	8.49		0.22
71	7.30	8.20		0.25
72	6.97	7.77		0.27
73	7.04	7.73		0.29
74	6.90	7.07		0.36
75	6.81	6.91	−4.07	0.36
76	6.82	7.49	−7.60	0.28
77	6.69	7.52		0.26
78	6.48	7.42		0.22
79	6.43	7.64		0.18
80	6.26	6.89		0.30
81	6.03	6.02		0.46
82	6.06	5.63		0.60
83	6.28	5.72		0.56
84	6.53	7.27		0.25
85	6.35	9.07		−0.02
86	5.98	8.50		0.005
87	5.73	7.12		0.21
88	5.61	5.32		0.65
89	5.85	4.79		0.77
90	5.96	5.35		0.64
91	5.87	6.15	−7.60	0.41

(B) *B-Salvo, 16 Nov. 1980*

Altitude (km)	Esrange (E9—075130 UT) H_p (km)	Esrange (E9—075130 UT) H_n (km)	Andøya (E4—033100 UT) H_i (km)	Esrange (E9—075130 UT) $\omega_B^2(\times 10^{-3}\,s^{-2})$
60	8.26	11.55	−2.97	0.004
61	7.81	12.26		−0.09
62	7.42	8.71		0.37
63	7.36	7.37		0.35
64	7.29	8.83		0.12
65	7.20	8.26		0.25
66	7.15	7.14		0.39
67	7.01	6.78		0.45
68	7.13	6.49		0.50
69	7.96	8.30		0.32
70	7.63	7.86		0.37
71	6.64	6.48	−2.97	0.38
72	7.12	8.46	−4.51	0.19
73	6.98	8.97		0.11
74	6.72	7.30		0.33
75	6.74	6.28		0.51
76	6.90	6.75		0.42
77	6.80	7.04		0.34
78	6.58	6.99		0.32
79	6.61	7.59		0.22
80	6.43	7.82		0.16
81	6.02	7.14	−4.51	0.19
82	5.93	7.05	−33.32	0.19
83	5.93	7.05		0.22
84	5.91	6.85		0.25
85	5.78	6.55		0.28
86	5.65	5.82		0.46
87	5.74	4.91		0.79
88	5.97	4.67		0.89
89	6.25	5.94		0.44
90	6.25	8.49		0.03
91	5.77	7.67	−33.32	0.11

(C) *A1-Salvo, 28 Nov. 1980*

Altitude (km)	Esrange (E9—032900 UT) H_p (km)	Esrange (E9—032900 UT) H_n (km)	Andøya (E4—032436 UT) H_i (km)	Esrange (E9—032900 UT) $\omega_B^2(\times 10^{-3}\,s^{-2})$
60	7.14	7.53	−2.89	0.36
61	7.16	6.65		0.52
62	7.05	6.64		0.39
63	7.06	7.30		0.33
64	7.25	6.63		0.56
65	7.44	6.04		0.67
66	7.30	6.91		0.43
67	7.29	7.96		0.26
68	7.60	8.00		0.32
69	8.37	9.01		0.28
70	7.48	7.72		0.37
71	6.55	6.09		0.46
72	7.36	7.93	−2.89	0.28
73	7.21	7.90	−38.40	0.27
74	7.03	7.38		0.33
75	7.25	7.43		0.37
76	7.26	7.16		0.43
77	7.00	6.49		0.51
78	6.99	6.07	−38.40	0.60
79	7.22	6.17	−5.95	0.58

(C) *A1-Salvo, 28 Nov. 1980—Continued*

Altitude (km)	Esrange (E9—032900 UT) H_p (km)	Esrange (E9—032900 UT) H_n (km)	Andøya (E4—032436 UT) H_i (km)	Esrange (E9—032900 UT) ω_B^2 ($\times 10^{-3}$ s^{-2})
80	7.26	6.67		0.46
81	6.96	7.43		0.25
82	6.85	8.66		0.08
83	6.81	9.56	−5.95	−0.02
84	6.87	10.36	−11.84	−0.06
85	6.68	9.30		0.03
86	6.38	7.01		0.33
87	6.40	5.46		0.68
88	6.63	5.38		0.75
89	6.86	6.23		0.51
90	6.78	7.31		0.32
91	6.70	9.29		0.004
92	6.49	14.86		−0.41
93	5.97	8.30	−11.84	0.06